International Journal for Modern Trends in Science and Technology
Volume 11, Issue 05, pages 1237-1247
ISSN: 2455-3778 online
Available online at: http://www.ijmtst.com/vol11issue05.html
DOI: https://doi.org/10.5281/zenodo.15511598

Performance Analysis of a Bidirectional Wireless Power Transfer System with Solar-Battery Input for EVs Using DPS-PWM

Rajesh.C[1], K.C. Satheesh[2], Dr. K. Siva Kumar [3]

[1]PG Student, Dept. of Electrical & Electronics Engineering, Sri Venkatesa Perumal College of Engineering and Technology, Puttur, Andhra Pradesh, India
[2]Assistant Professor, Dept. of Electrical & Electronics Engineering, Sri Venkatesa Perumal College of Engineering and Technology, Puttur, Andhra Pradesh, India
[3]Professor, Dept. of Electrical & Electronics Engineering, Sri Venkatesa Perumal College of Engineering and Technology, Puttur, Andhra Pradesh, India

To Cite this Article
Rajesh.C, K.C. Satheesh & Dr. K. Siva Kumar (2025). Performance Analysis of a Bidirectional Wireless Power Transfer System with Solar-Battery Input for EVs Using DPS-PWM. International Journal for Modern Trends in Science and Technology, 11(05), 1237-1247. https://doi.org/10.5281/zenodo.15511598

Article Info
Received: 27 April 2025; Accepted: 22 May 2025.; Published: 25 May 2025.

KEYWORDS

Bidirectional Wireless Power Transfer, Electric Vehicle Charging, Solar Energy, incremental conductance (INC) MPPT, LCC Compensation Topology, Dual Phase Shift PWM (DPS-PWM), Battery Energy Storage, Vehicle-to-Battery (V2B)

ABSTRACT

This paper presents a solar and battery-powered bidirectional wireless power transfer (BWPT) system designed for efficient electric vehicle (EV) charging using a dual phase shift pulse width modulation (DPS-PWM) control technique. The system integrates a solar photovoltaic (PV) array with a boost converter employing a incremental conductance (INC) maximum power point tracking (MPPT) algorithm to maximize solar power extraction under varying irradiance conditions. An LCC compensation topology is utilized to enhance power transfer efficiency and system stability during contactless energy transmission. The DPS-PWM method independently regulates the phase shifts of the primary and secondary converters, enabling precise bidirectional power flow control between the solar source, battery energy storage system (BESS), and the EV charging load. Under sufficient solar irradiation, power is supplied simultaneously to charge the battery and EV, while the battery provides backup energy during low solar conditions, ensuring uninterrupted EV charging. The system also supports reverse power flow from the EV back to the battery, facilitating vehicle-to-battery (V2B) operation. Simulation results at an operating frequency of 85 kHz and rated power of 3.7 kW demonstrate a high power transfer efficiency of approximately 94.4%, validating the system's effectiveness for fast, reliable, and contactless

bidirectional wireless EV charging powered by renewable energy. The proposed integration of MPPT, LCC compensation, and DPS-PWM control offers a flexible and efficient solution for modern EV charging infrastructure.

1. Introduction

Electric vehicles (EVs) are gaining significant attention worldwide as a sustainable alternative to conventional internal combustion engine vehicles, contributing to reduced carbon emissions and improved air quality. The development of efficient, reliable and user-friendly charging infrastructure is critical to supporting the widespread adoption of EVs. Wireless power transfer (WPT) technology has emerged as a promising solution for EV charging by enabling contactless energy transfer. This approach improves convenience, enhances safety by eliminating physical connectors, and reduces wear and tear associated with plug-in chargers [1], [2]. Among WPT technologies, bidirectional wireless power transfer (BWPT) systems allow energy flow in both directions, from the charging source to the vehicle (Grid to Vehicle, G2V) and from the vehicle back to the energy storage or load (Vehicle to Grid, V2G, or Vehicle to Battery, V2B). This bidirectional capability facilitates energy management, load leveling, and emergency power supply scenarios [3], [4]. In wireless power transfer applications, several resonant topologies have been explored to optimize efficiency and power density. The LCC compensation topology is widely used due to its inherent resonance, which reduces switching losses and improves system robustness. Recently, the LCC-based Bidirectional Wireless Power Transfer (LCC-BWPT) system has gained interest for EV charging applications, offering stable and efficient power transfer with simplified tuning requirements [5], [6]. However, despite its advantages, LCC-BWPT systems can face challenges such as limited dynamic control range and sensitivity to parameter variations, which may impact system performance under rapidly changing load or input conditions. Traditional bidirectional power conversion for EV charging has also been realized using DC-DC converters, such as buck-boost topologies. While bidirectional DC-DC buck-boost converters can effectively manage power flow between the battery and load, they have several limitations when applied to EV wireless charging systems. These converters typically require complex control schemes to handle both power directions and often suffer from lower efficiency due to multiple energy conversion stages. Additionally, DC-DC converters are generally limited by the physical constraints of wired connections, reducing the convenience and flexibility that wireless systems offer [7], [8]. In contrast, bidirectional wireless power transfer systems combine the advantages of contactless energy transmission with bidirectional power flow capability, improving system flexibility and user experience. Nonetheless, controlling BWPT systems effectively is complex due to the need for dual-side power converter control to ensure efficient energy transfer during both charging and discharging cycles. Conventional control methods for unidirectional WPT are inadequate for BWPT applications because of these added complexities [9]. To address these challenges, this work proposes a dual phase shift pulse width modulation (DPS-PWM) control technique applied to a bidirectional wireless power transfer system operating at a high frequency of 85 kilohertz and rated at 3.7 kilowatts. The proposed control strategy enables independent phase shift adjustment of both primary and secondary converters, allowing precise regulation of power flow direction and magnitude between the solar photovoltaic system, battery energy storage, and EV charging load. In this system, solar panels generate power to simultaneously charge the battery and supply the EV charger during periods of sufficient solar irradiation. When solar energy availability decreases, the battery provides backup power to maintain continuous EV charging. Additionally, the system supports reverse power flow from the EV to the battery, facilitating efficient vehicle-to-battery energy transfer and enhancing overall system flexibility and energy management [10], [11]. Simulation results demonstrate that the DPS-PWM control technique achieves high power transfer efficiency of approximately 94.4%, significantly improving fast and reliable bidirectional wireless power transfer. Unlike previous bidirectional DC-DC converters that rely on wired connections and suffer from conversion losses, the proposed BWPT system offers contactless energy transfer with reduced power losses and improved convenience. Compared to the LCC-BWPT topology, the DPS-PWM approach provides enhanced dynamic control and flexibility, addressing parameter sensitivity issues and enabling efficient

operation under varying solar and load conditions. This makes the proposed system particularly well-suited for off-grid or remote locations where consistent and flexible EV charging is necessary [12], [13]. The integrating solar energy, battery storage, and bidirectional wireless power transfer with advanced DPS-PWM control offers a comprehensive and efficient solution for modern EV charging infrastructure. This system promotes renewable energy utilization, enhances user convenience through wireless operation, and improves overall energy management flexibility. The main features of the proposed configuration are as follows.

- Enables two-way power flow between the battery and EV (Battery to EV and EV to Battery) without physical connectors, improving user convenience and flexibility.
- An MPPT control of incremental conductance (INC) effectively harvested the PV array maximum power.
- Stores surplus solar energy and supplies backup power to the EV charging system when solar irradiation is insufficient.
- Allows independent control of primary and secondary side converters, ensuring precise regulation of power direction and magnitude for efficient operation.
- Employs LCC resonance on both transmitter and receiver sides to minimize switching losses, enhance voltage gain, and maintain system stability.
- Supports compact coil design, reduced system size, and improved power density while enabling high-frequency resonant operation.
- Achieves a simulated power transfer efficiency of up to 94.4%, facilitating quick and reliable EV charging.
- Eliminates mechanical wear and enhances safety by avoiding physical plug-in connections, making the system suitable for both indoor and outdoor EV charging stations.

2. System Configuration

The system consists of a solar photovoltaic (PV) array, a battery energy storage system (BESS), and an electric vehicle (EV) charging load connected through a bidirectional wireless power transfer (BWPT) setup employing an LCC compensation topology and controlled by a dual phase shift pulse width modulation (DPS-PWM) technique as shown in Fig.1. The solar panels generate power to charge the battery and supply the EV charger when sunlight is available. When solar irradiation decreases, the battery provides backup power to maintain continuous EV charging. The system also supports reverse power flow, allowing energy from the EV to charge the battery, enabling bidirectional operation. The LCC compensation network enhances the power transfer efficiency by providing resonant conditions that reduce switching losses and improve system stability during wireless energy transfer at an operating frequency of 85 kHz and a power rating of 3.7 kW. Dual converters on both sides, controlled independently by the DPS-PWM technique, allow precise regulation of power flow direction and magnitude, enabling fast and efficient charging and discharging cycles. This configuration improves overall energy management, increases system flexibility, and eliminates the need for physical connectors, making it well-suited for advanced EV charging infrastructure integrating renewable energy sources.

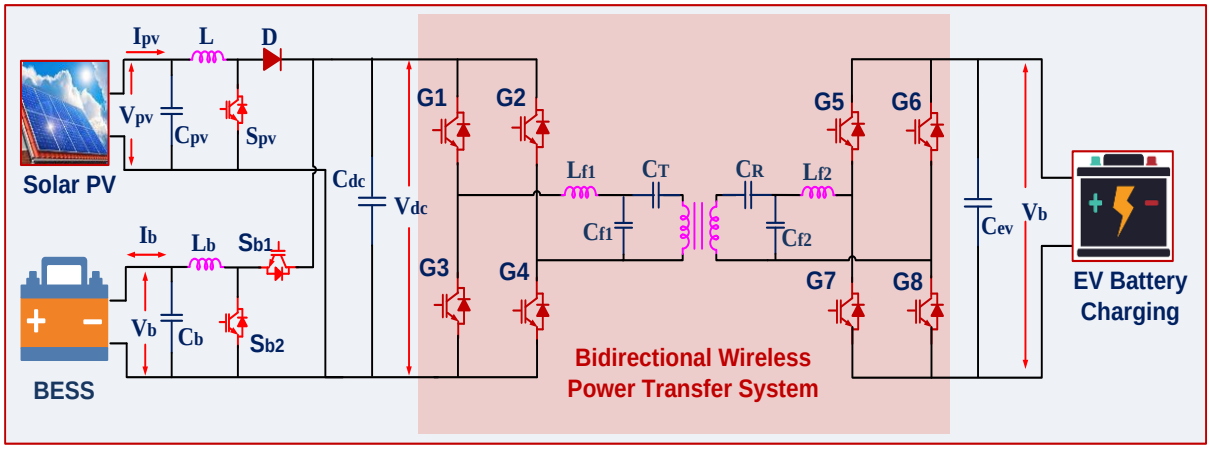

Fig.1 proposed system configuration

3. Modeling and Designing of Proposed System Configuration

A. Solar PV system

The single diode model effectively captures the behavior of a solar cell under various environmental conditions such as temperature and solar irradiance. When sunlight strikes the solar cell, it generates a photocurrent Iph, which increases proportionally with solar irradiance and slightly varies with temperature. The diode represents the p-n junction within the cell and accounts for recombination losses, while the series resistance Rs models internal resistive losses, and the shunt resistance Rsh accounts for leakage currents. The output current I is determined by the difference between the photo-generated current and the diode leakage current, adjusted for voltage drops across resistances. This equation is nonlinear and must often be solved iteratively for accurate simulation or design. By adjusting the operating voltage V, the solar cell can operate at different points on its I-V curve. At open circuit, the current is zero, and at short circuit, the voltage is zero. Between these extremes lies the Maximum Power Point (MPP), where the product of current and voltage (power) is highest, representing the most efficient operating point of the PV cell. In practical PV systems, Maximum Power Point Tracking (MPPT) algorithms, such as Incremental Conductance or Perturb & Observe, dynamically adjust the load or converter duty cycle to maintain the operating point near the MPP despite changes in sunlight intensity or temperature. This maximizes the harvested energy. The single diode model provides a reliable and widely used framework for understanding, simulating, and designing PV systems, allowing engineers to predict performance under diverse conditions and optimize system components like DC-DC converters and energy storage.

a. Single Diode Model of a PV Cell

The single diode model is widely used to represent the electrical behavior of a solar cell or PV module, capturing its nonlinear current-voltage (I-V) characteristics.

1. Equivalent Circuit: A current source Iph in parallel with a diode (with saturation current I0), series resistance Rs, and shunt resistance Rsh.

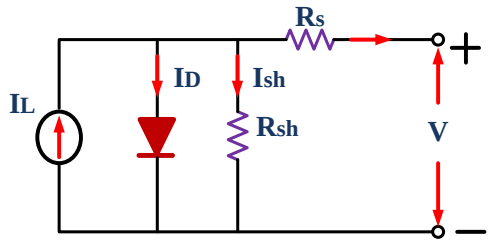

Fig. 2 equivalent model of PV solar.

2. Output Current Equation:

$$I = I_{ph} - I_0\left(e^{\frac{q(V+IR_S)}{nkT}-1}\right) - \frac{V+IR_S}{R_{sh}} \qquad (1)$$

Where:

- I = output current (A)
- V = output voltage (V)
- Iph = photo-generated current (A)
- I0 = diode saturation current (A)
- q = electron charge 1.602×10−19 C)
- n = diode ideality factor (typically 1 to 2)
- k = Boltzmann constant 1.381×10−23 J/K
- T = cell temperature (Kelvin)
- Rs = series resistance (Ω)
- Rsh = shunt resistance (Ω)

3. Photo-generated current Iph:

$$I_{ph} = \left[I_{sc} + K_i(T - T_{ref})\right] \times \frac{G}{G_{ref}} \qquad (2)$$

Where:

- Isc = short-circuit current at reference temperature
- Ki = temperature coefficient of current (A/°C)
- Tref = reference temperature (usually 25°C or 298 K)
- G = solar irradiance (W/m²)
- Gref = reference irradiance (1000 W/m²)

4. Diode Saturation Current I0:

$$I_0 = I_{0_{ref}}\left(\frac{T}{T_{ref}}\right)^3 \exp\left(\frac{qE_g}{nk}\left(\frac{1}{T_{ref}} - \frac{1}{T}\right)\right) \qquad (3)$$

Where:

- I0ref = diode saturation current at Tref
- Eg = bandgap energy of the semiconductor (eV)

5. Open-circuit voltage Voc:

$$V_{oc} = \frac{nkT}{q} In\left(\frac{I_{ph}}{I_0} + 1\right) \qquad (4)$$

B. Solar PV boost Converter

The boost converter is a DC-DC converter designed to step up the input voltage to a higher output voltage level as shown in Fig.3. It mainly consists of four components: an inductor (L), a switch (usually a MOSFET), a diode (D), and an output capacitor (C). During the ON state, the MOSFET switch is closed, allowing current to flow from the photovoltaic (PV) panel through the inductor. This causes energy to be stored in the magnetic field of the inductor while the diode remains reverse biased, preventing current from reaching the output. When the switch turns OFF, the MOSFET opens, and the inductor's magnetic field collapses, releasing the stored energy. The inductor current then flows through the diode to the output capacitor and load, effectively adding to the input voltage. This process results in an output voltage that is higher than the input voltage, enabling efficient voltage boosting suitable for charging batteries or powering loads.

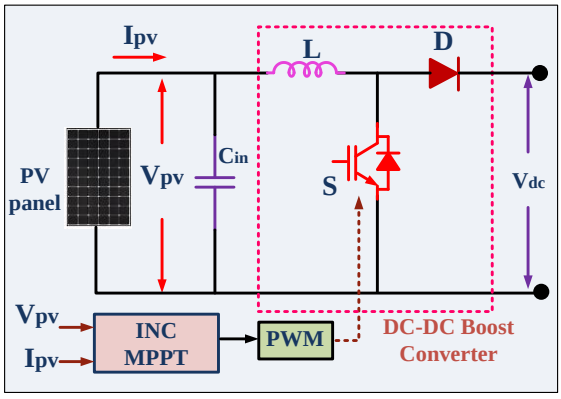

Fig. 3 solar PV INC MPPT DC-DC boost converter

1. Output Voltage of Boost Converter

$$V_o = \frac{V_{in}}{1-D} \quad (5)$$

Where: Vo: Output voltage, Vin: PV input voltage, D: Duty cycle (0 < D < 1)

2. Inductor Value (L)

$$L = \frac{V_{in} \cdot D}{f_s \cdot \Delta I_L} \quad (6)$$

Where:

- fs: Switching frequency (Hz)
- ΔIL: Inductor ripple current (A), usually 20–40% of Iin

3. Output Capacitor Value (C)

$$C = \frac{I_o \cdot D}{f_s \cdot \Delta V_o} \quad (7)$$

Where: Io: Output current (A), ΔVo: Acceptable output voltage ripple (V)

C. MPPT Control

Fig. 4 depicts the solar PV array's greatest power point technique. It generates a voltage reference (V*pv) that is the same as the MPP voltage of the PV array.

At the MPP,

$$\frac{dP_{PV}}{dV_{PV}} = 0 \quad (8)$$

$$\frac{d(V_{PV}I_{PV})}{dV_{PV}} = I_{PV} + V_{PV}\frac{dI_{PV}}{dV_{PV}} = 0 \quad (9)$$

$$\frac{dI_{PV}}{dV_{PV}} = -\frac{I_{PV}}{V_{PV}} \quad (10)$$

Right side displays PV array instantaneous conductance. Conditions of INC MPPT control:

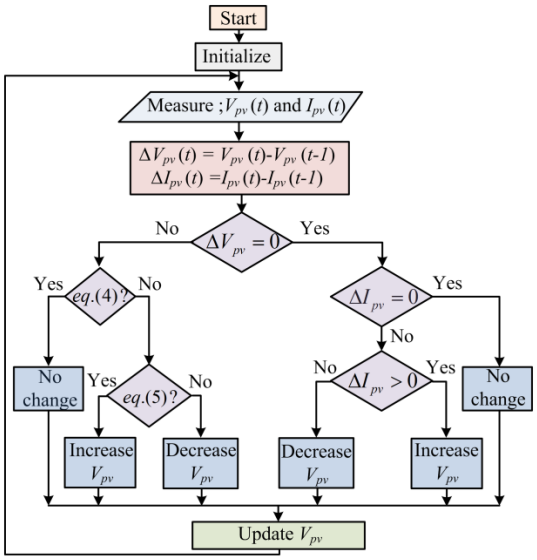

Fig. 4 INC MPPT control

$$\frac{dI_{PV}}{dV_{PV}} = -\frac{I_{PV}}{V_{PV}}\left(\frac{dP_{PV}}{dV_{PV}} = 0, \text{at MPP}\right) \quad (11)$$

$$\frac{dI_{PV}}{dV_{PV}} > -\frac{I_{PV}}{V_{PV}}\left(\frac{dP_{PV}}{dV_{PVg}} > 0, \text{at left of MPP}\right) \quad (12)$$

$$\frac{dI_{PV}}{dV_{PV}} < -\frac{I_{PV}}{V_{PV}}\left(\frac{dP_{PV}}{dV_{PV}} < 0, \textit{at right of MPP}\right) \quad (13)$$

According to the circumstances, the disturbance arises in the PV array's voltage, which is used to monitor the array's maximum power point.

4. Designing Battery Energy Storage System

The bidirectional buck-boost converter plays a crucial role in managing energy flow between the battery energy storage system (BESS) and the DC bus in a microgrid. This converter enables both charging and discharging of the battery, ensuring stable power delivery for electric vehicle (EV) charging. In buck mode, the converter steps down the DC bus voltage to charge the battery, while in boost mode, it steps up the battery voltage to supply power to the microgrid or EV load as shown in Fig.5. The control strategy dynamically adjusts the duty cycle to regulate power flow efficiently. The converter also helps stabilize the DC bus voltage,

mitigating fluctuations from intermittent renewable energy sources like solar and wind. The energy management strategy ensures optimal charging and discharging cycles, enhancing battery lifespan and overall system efficiency.

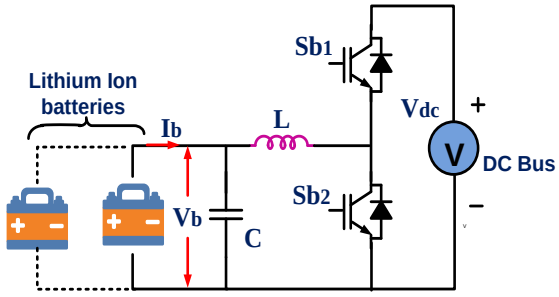

Fig.5 principle operation bidirectional dc-dc buck boost converter

1. Buck Mode (Battery Charging)

Output Voltage in Buck Mode:

$$V_b = D \cdot V_{dc} \quad (14)$$

Where: Vb = Battery voltage, Vdc = DC bus voltage, D = Duty cycle (0<D<1)

Inductor Current Ripple in Buck Mode:

$$\Delta I_L = \frac{(1-D)V_{dc}}{Lf_S} \quad (15)$$

Where: ΔIL = Inductor current ripple, L = Inductor value, fs = Switching frequency

2. Boost Mode (Battery Discharging)

Output Voltage in Boost Mode:

$$V_{dc} = \frac{V_b}{1-D} \quad (16)$$

Inductor Current Ripple in Boost Mode:

$$\Delta I_L = \frac{DV_b}{Lf_S} \quad (17)$$

A. Double-Loop Controller for EV Charging System

The control strategy for electric vehicle (EV) charging involves a double-loop control system to ensure efficient, stable, and safe charging as shown in Fig.6. The outer voltage loop maintains a constant DC bus voltage, while the inner current loop regulates the battery charging current. A Proportional-Integral (PI) controller is used in both loops to minimize steady-state error and improve dynamic performance.

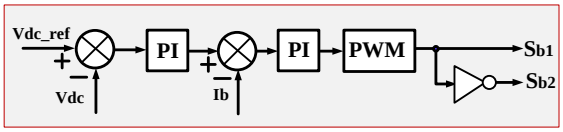

Fig. 6 double loop ev charging controller

1. Outer Voltage Loop: DC Bus Voltage Control

The outer voltage loop ensures the DC bus voltage (Vdc) remains stable and within the desired range. Since variations in EV charging loads and grid fluctuations affect the DC bus voltage, this loop provides a reference current (Iev∗) for the inner current loop.

Error Signal Calculation:

$$e_v(t) = V_{dc}^* - V_{dc} \quad (18)$$

PI Controller Output (Reference EV Charging Current Iev∗)

$$I_{ev}^*(t) = K_{Pv}e_v(t) + k_{iv}\int e_v(t)\,dt \quad (19)$$

Where: Iev∗= Reference charging current for the inner loop, Kpv= Proportional gain of voltage controller, Kiv= Integral gain of voltage controller

This reference current is then passed to the inner current loop for precise battery charging control.

2. Inner Current Loop: Battery Current Control

The inner current loop ensures the EV battery is charged with a smooth and regulated current to prevent over current issues and battery degradation. The PI controller in this loop generates the duty cycle for the DC-DC converter (buck or boost).

Error Signal Calculation:

$$e_i(t) = I_{ev}^* - I_{ev} \quad (20)$$

PI Controller Output (Duty Cycle Control)

$$D(t) = K_{Pi}e_i(t) + k_{ii}\int e_i(t)\,dt \quad (21)$$

Where: D = Duty cycle of the DC-DC converter, Kpi= Proportional gain of current controller, Kii= Integral gain of current controller

This duty cycle (D) is applied to the DC-DC converter, adjusting the output voltage and current to regulate battery charging.

5. Designing of the BWPT System

The design of the Bidirectional Wireless Power Transfer (BWPT) system centers on developing a phase shift controller to improve power factor correction (PFC) and optimize power transfer efficiency between the primary and secondary coils at the resonance frequency as shown in Fig.7. The power transfer depends on the mutual inductance (M), which is influenced by coil size, turns, and air gap, with higher coupling coefficients (K) achieved by larger pad diameters and smaller air gaps, enhanced further by ferrite cores. The system operates at 85 kHz, following the SAE J2954 standard, and incorporates LCC-LCC compensation circuits for both primary and secondary coils, providing greater flexibility in controlling coil currents and voltage levels. The coil currents are directly affected by the compensating inductances, which must be carefully

selected to balance current reduction against increased coil voltage that could impact safety and reliability. Coil voltage and current relationships are quantified by equations involving coil turns, inductance per turn, and the compensation inductors. After defining the coil design, capacitors for the resonant circuit are calculated based on the resonance frequency to ensure optimal operation. The design also considers electrical, magnetic, and thermal factors, including the ferrite core width and Litz wire specifications, to avoid excessive core losses and maintain component integrity. Finally, voltages and currents in the resonant tank components are computed to meet operational requirements while observing heating and safety constraints for high-frequency, high-power capacitors.

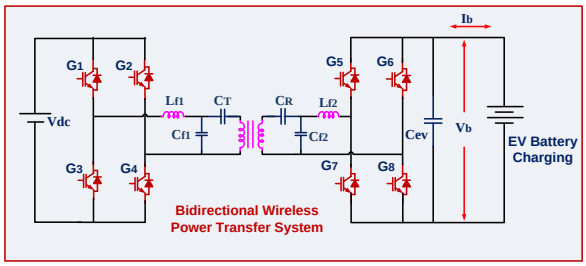

Fig.7 Bidirectional Wireless Power Transfer for EV charging system

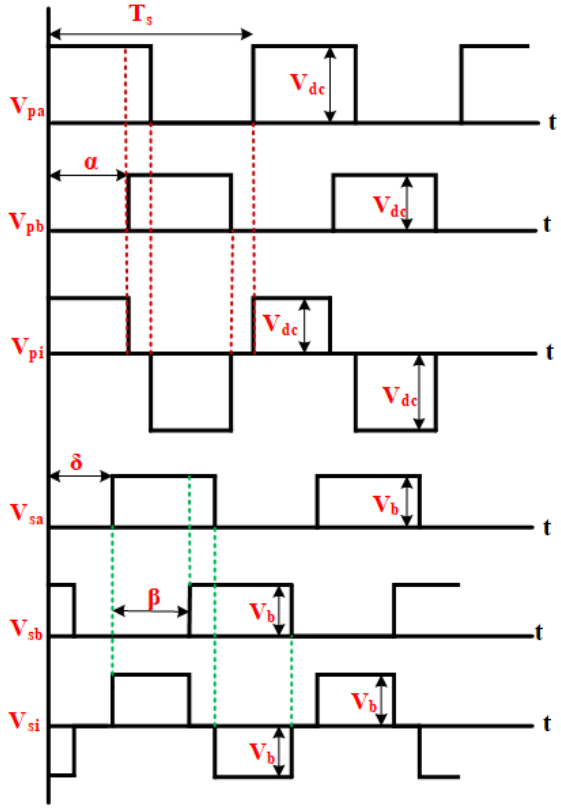

Fig 8. Switching waveforms of phase angle delay between the two converters.

The design of the Bidirectional Wireless Power Transfer(BWPT) system focuses on efficient power transfer between the primary and secondary coils at the resonance frequency, which can be expressed as:

$$P = \omega_0 M I_p I_s \qquad (22)$$

where ω0 is the angular resonance frequency, M is the mutual inductance between the coils, and Ip, Is are the RMS currents in the primary and secondary coils, respectively. The mutual inductance M depends on the coupling coefficient K and the self-inductances of the coils:

$$M = K\sqrt{L_p L_s} \qquad (23)$$

Here, Lp and Ls are the self-inductances of the primary and secondary coils, and K is influenced by coil size, spacing (air gap), and the presence of ferrite cores which improve coupling by 30%-50%. The output power is also given by:

$$P = 2\pi f_0 (N_p I_p)(N_s I_s) K \sqrt{\hat{L}_p \hat{L}_s} \qquad (24)$$

where f0 is the operating frequency (85 kHz), Np and Ns are the number of turns in primary and secondary coils, and L^p, L^s are inductances per turn.

Using LCC-LCC compensation circuits enhances system control and efficiency. The coil currents relate to input voltages VAB and compensating inductors L11, L22 as:

$$I_p = \frac{V_{AB}}{\omega_0 L_{11}}$$

$$I_s = \frac{V_{ab}}{\omega_0 L_{22}} \qquad (25)$$

Adjusting L11 can reduce primary coil current, but increasing coil turns also raises coil inductance and voltage, limited by insulation and safety constraints. Coil voltages are calculated by:

$$V_{L_p} = I_p X_{L_p} = j\omega L_p I_p = I_P\left(2\pi N_p^2 \hat{L}_p\right) \qquad (26)$$

$$V_{L_s} = I_s X_{L_s} = j\omega L_s I_s = I_s\left(2\pi N_s^2 \hat{L}_s\right) \qquad (27)$$

The voltage gain ratio between coil voltage and input voltage is:

$$G_{vp} = \frac{V_{Lp}}{V_{AB}} = \frac{X_{Lp}}{X_{L_{11}}} = \frac{L_p}{L_{11}} \qquad (28)$$

The resonance frequencies for the LCC compensation tanks are given by:

$$\omega_0 = \frac{1}{\sqrt{L_{11} C_{11}}} = \frac{1}{\sqrt{(L_p - L_{11}) C_{12}}} \qquad (29)$$

$$\omega_0 = \frac{1}{\sqrt{L_{22} C_{22}}} = \frac{1}{\sqrt{(L_S - L_{22}) C_{21}}} \qquad (30)$$

Currents through the resonant tank's tuning inductors and coils are:

$$I_{L_{11}} = \frac{M V_{AB}}{\omega_0 L_{11} L_{12}} \qquad (31)$$

$$I_{L_{22}} = \frac{M V_{ab}}{\omega_0 L_{11} L_{22}} \qquad (32)$$

$$I_{L_p} = \frac{V_{AB}}{\omega_0 L_{11}} \quad (33)$$

$$I_{L_s} = \frac{V_{ab}}{\omega_0 L_{22}} \quad (34)$$

Voltages across the tuning capacitors are:

$$V_{C_{12}} = V_{AB} \frac{(L_p - L_{11})}{L_{11}} \quad (35)$$

$$V_{C_{21}} = V_{ab} \frac{(L_s - L_{22})}{L_{22}} \quad (36)$$

The design involves balancing coil turns, inductance, and compensation capacitances to ensure efficient power transfer, stable resonance, and adherence to voltage and current limits imposed by the components and safety requirements.

6. CONTROL ALGORITHM

The proposed system is designed for the maximum power of 10KW having a rated voltage of solar PV bidirectional DC-DC charging station. The SPV array is designed and installed to supply the electric vehicle loads during this mode. A 10 kW SPV array is installed on the charging station which supplies to the electric vehicle battery for the residential, home, offices and public charging applications. V2V mode: In B2V mode there is simultaneously charging and discharging process will happen, so for this to be successfully done the single phase shift current control algorithm is used. The mathematical formulation of the controller can be explained as:

Modeling of the Controller:

The battery current error is given as:

$$I_b^*(t) - I_{b1}(t) = e(t) \quad (37)$$

Where Ib*(t) is reference value of battery current, Ib1(t) is the main battery current and e(t) is the error signal generated. This error signal is passed through PI controller whose transfer function is given as:

$$e(t) \times K_P + e(t) \times \frac{K_i}{s} = u(a) \quad (38)$$

For proper designed value of Ki and Kp, an output signal is generated, which is multiplied by the constant α. Where α is taken as,

$$\alpha = 0.5 \times \frac{1}{85000} \quad (39)$$

Where 1/85000 is the switching time period

The signal obtained in equation (39) acts as a delay for the second bridge with respect to the first bridge of the converter which is shown in Fig.6. The value of the delay is varying between 4μs to 5μs and hence according to this delay, power varies at the output. The charging and discharging control strategy is shown in Fig.9 and Fig. 10 respectively. The charging and discharging switching operations can be understood by the switching wave forms which is presented in Fig.11.

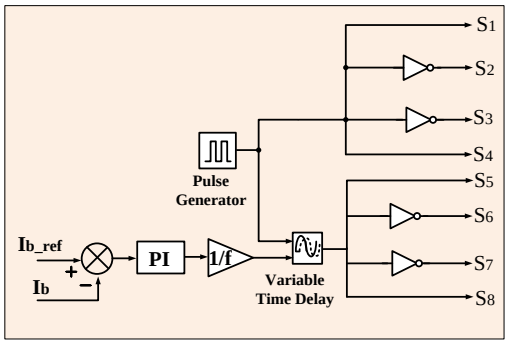

Fig.9 DAB charging algorithm

Discharging Mode:

For the discharging mode the similar technique is used. The reference current is added to the auxiliary battery current and

$$I_b^*(t) - I_{b2}(t) = e_a(t) \quad (40)$$

Switching pulse is also reversed in order to reverse the power flow. The mathematical formulation of discharging controller is given as,

$$e_b(t) \times K_p + e_b(t) \times \frac{K_i}{s} = u(b) \quad (41)$$

The u(b) signal is again multiplied with the constant value α and generated u(ref2), where α value is taken as:

$$\alpha = 0.5 \times \frac{1}{85000} \quad (42)$$

Where $\frac{1}{85000}$ is the switching time period now u (ref2) is acting as a delay to the primary bridge of the DAB converter with respect to the secondary bridge of converter and hence power is now transferred from secondary bridge side to primary bridge side

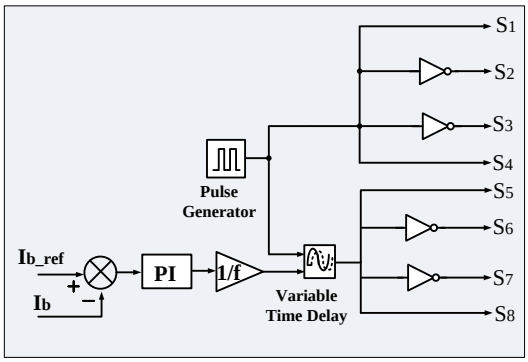

Fig.10 DAB discharging algorithm

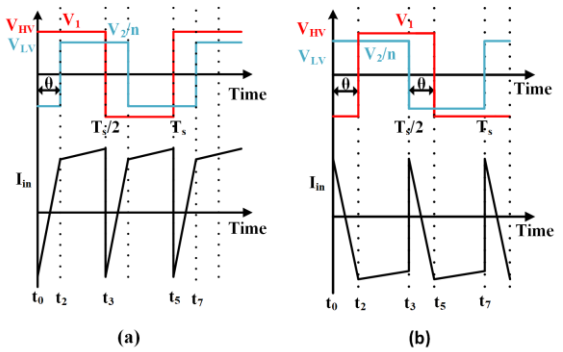

Fig. 11 (a) Voltage and input current waveforms in forward power flow; (b) Voltage and input current waveforms in reverse power flow

7. Simulation Results and Discussion

A. Dynamic Performance Evaluation of the Hybrid Solar-Battery Bidirectional Wireless Power Transfer System for EV Charging under Variable Irradiance

The proposed system consists of a 10 kW solar photovoltaic (PV) array, a 6.5 kW battery energy storage system (BESS), and a 5 kW electric vehicle (EV) battery. The solar array is connected to both the BESS and the EV battery through a DC-DC bidirectional buck-boost converter and a bidirectional wireless power transfer (BWPT) system, respectively. The total simulation duration is 1 second, with varying solar irradiation conditions. From 0 to 0.2 seconds, the solar irradiation is constant at 1000 W/m², generating a peak solar power of Psolar=10kW. During this period, the PV system supplies energy directly to both the BESS and the EV battery. The EV battery charges at a constant rate of approximately PEV=4.5kW, while the remaining PBESS=10 kW−4.5 kW=5.5kW is used to charge the BESS. From 0.2 to 0.3 seconds, the solar irradiation decreases linearly from 1000 W/m² to 500 W/m², leading to a corresponding drop in power output from 10 kW to 5 kW, calculated using the proportional relation P=η·A·G, where η is efficiency, A is panel area, and G is irradiation. Despite this decrease, the system continues to charge the EV battery with 4.5 kW, utilizing the available solar energy and compensating for the deficit from the partially charged BESS. This coordinated power-sharing highlights the dynamic energy balancing between PV and battery sources. From 0.3 to 0.4 seconds, the solar irradiation further drops from 500 W/m² to 0, reducing the PV output from 5 kW to 0 kW. As no power is generated by the PV during this interval, the BESS discharges to supply the full charging demand of the EV battery at 4.5 kW. Given the BESS rated capacity of 6.5 kW, the discharging is within operational limits, demonstrating the BESS's capability to maintain load support during solar power outages. From 0.4 to 0.5 seconds, the solar output remains zero, and the BESS continues to supply 4.5 kW to the EV battery uninterruptedly. This reflects the system's effective backup mechanism via stored energy. Between 0.5 and 0.7 seconds, no energy transfer takes place, and both the EV battery and BESS remain idle. This phase acts as a buffer, maintaining energy equilibrium in the system. From 0.7 to 1.0 seconds, the direction of power flow reverses, and the EV battery begins discharging at 4.5 kW to charge the BESS. This bidirectional interaction is enabled by the wireless power interface and buck-boost control, with energy transfer satisfying E=P·t=4.5kW. This final phase showcases the flexibility and robustness of the proposed system, ensuring that energy is redistributed as needed for maintaining system stability and enhancing energy utilization as shown in Fig.12.

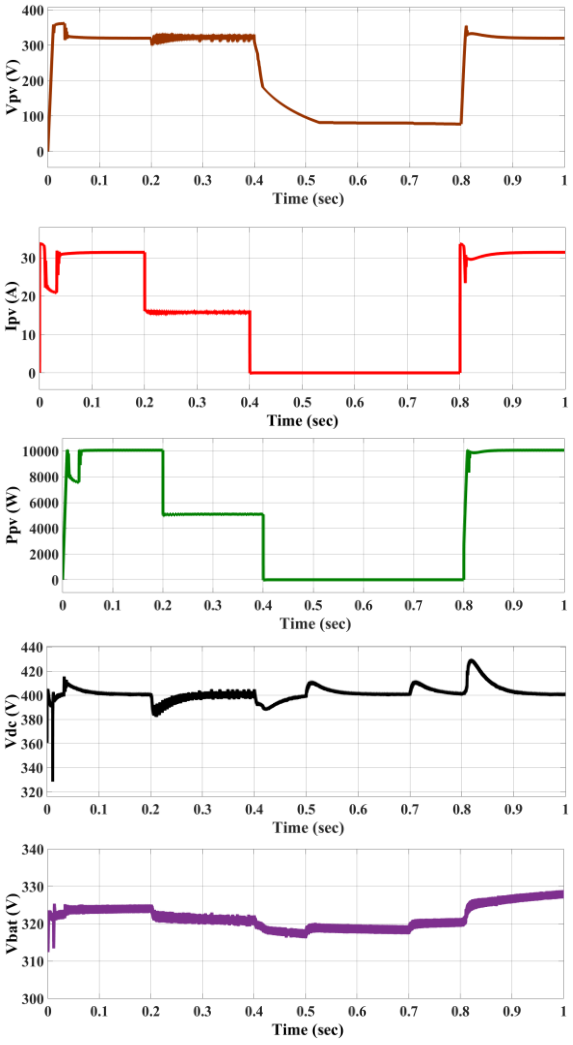

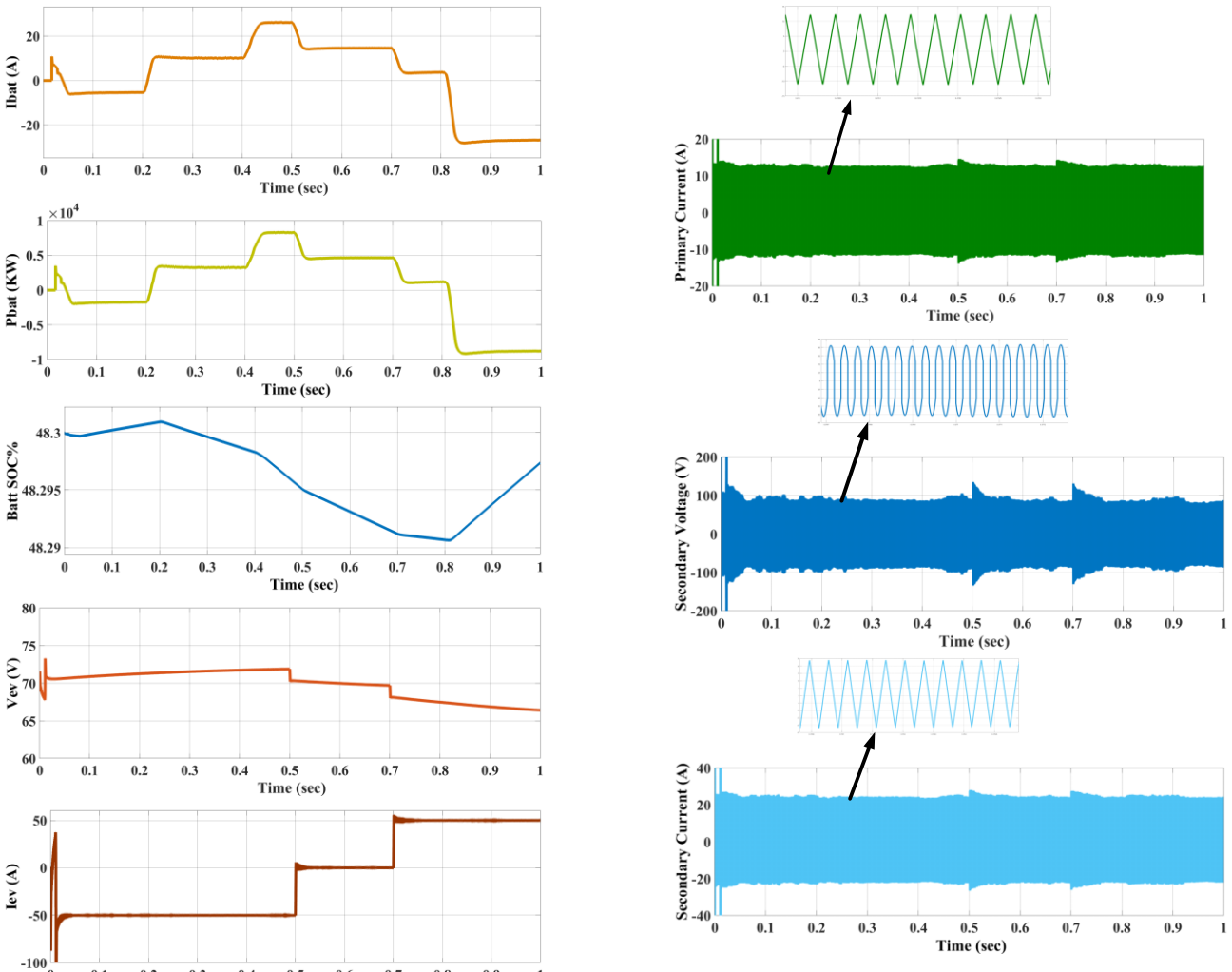

Fig.12 Simulation results of the Hybrid Solar-Battery Bidirectional Wireless Power Transfer System for EV Charging under Variable Irradiance Conditions

8. Conclusion

This paper presents a high-efficiency bidirectional wireless power transfer (BWPT) system integrating solar photovoltaic (PV) energy and a battery energy storage system (BESS) for electric vehicle (EV) charging. The proposed system employs an LCC compensation topology to ensure stable and efficient contactless energy transfer, while a dual phase shift pulse width modulation (DPS-PWM) control technique enables precise and flexible power flow regulation between the solar source, battery, and EV. Simulation results demonstrate that the system achieves a notable power transfer efficiency of approximately 94.4% at an operating frequency of 85 kHz and a rated power of 3.7 kW. The integration of the incremental conductance (INC) MPPT algorithm maximizes solar energy extraction under dynamic irradiance conditions, ensuring optimal system performance. Furthermore, the

system supports bidirectional energy flow, including vehicle-to-battery (V2B) operation, enhancing the flexibility of energy management. Overall, the proposed BWPT system offers a reliable, contactless, and renewable energy-based solution for modern EV charging infrastructure, particularly suitable for off-grid and remote applications where flexible, efficient, and sustainable energy solutions are essential.

Conflict of interest statement

Authors declare that they do not have any conflict of interest.

REFERENCES

[1] I. Kougioulis, A. Pal, P. Wheeler, and M. R. Ahmed, "An isolated multiport DC–DC converter for integrated electric vehicle on-board charger," IEEE J. Emerg. Sel. Topics Power Electron., vol. 11, no. 4, pp. 4178–4198, Aug. 2023.

[2] H. Qari, S. Khosrogorji, and H. Torkaman, "Optimal sizing of hybrid WT/PV/diesel generator/battery system using MINLP method for a region in Kerman," Scientia Iranica, vol. 27, no. 6, pp. 3066–3074, 2020.

[3] H. Heydari-Doostabad and T. O'Donnell, "A wide-range high-voltagegain bidirectional DC–DC converter for V2G and G2 V hybrid EV charger," IEEE Trans. Ind. Electron., vol. 69, no. 5, pp. 4718–4729, May 2022.

[4] M. A. H. Rafi and J. Bauman, "Optimal control of semi-dual active bridge DC/DC converter with wide voltage gain in a fast-charging station with battery energy storage," IEEE Trans. Transport. Electrific., vol. 8, no. 3, pp. 3164–3176, Sep. 2022.

[5] X. Qu, H. Chu, S.-C. Wong, and C. K. Tse, ''An IPT battery charger with near unity power factor and load-independent constant output combating design constraints of input voltage and transformer parameters,'' IEEE Trans. Power Electron., vol. 34, no. 8, pp. 7719–7727, Aug. 2019.

[6] X. Liu, N. Jin, X. Yang, K. Hashmi, D. Ma, and H. Tang, ''A novel singleswitch phase controlled wireless power transfer system,'' Electronics, vol. 7, no. 11, p. 281, Oct. 2018.

[7] V. Shevchenko, O. Husev, R. Strzelecki, B. Pakhaliuk, N. Poliakov, and N. Strzelecka, ''Compensation topologies in IPT systems: Standards, requirements, classification, analysis, comparison and application,'' IEEE Access, vol. 7, pp. 120559–120580, 2019.

[8] D. Xu, C. Zhao, and H. Fan, ''A PWM plus phase-shift control bidirectional DC–DC converter,'' IEEE Trans. Power Electron., vol. 19, no. 3, pp. 666–675, May 2004.

[9] R. Bosshard, J. W. Kolar, J. Mühlethaler, I. Stevanovic, B. Wunsch, and F. Canales, ''Modeling and η–α -Pareto optimization of inductive power transfer coils for electric vehicles,'' IEEE J. Emerg. Sel. Topics Power Electron., vol. 3, no. 1, pp. 50–64, Mar. 2015.

[10] R. Bosshard and J. W. Kolar, ''Inductive power transfer for electric vehicle charging: Technical challenges and tradeoffs,'' IEEE Power Electron. Mag., vol. 3, no. 3, pp. 22–30, Sep. 2016.

[11] P. He and A. Khaligh, "Comprehensive analyses and comparison of 1 kW isolated DC–DC converters for bidirectional EV charging systems," IEEE Trans. Transport. Electrific., vol. 3, no. 1, pp. 147–156, Mar. 2017.

[12] M. Mohammad, O. C. Onar, G.-J. Su, J. Pries, V. P. Galigekere, S. Anwar, E. Asa, J. Wilkins, R. Wiles, C. P. White, and L. E. Seiber, ''Bidirectional LCC–LCC-compensated 20-kW wireless power transfer system for medium-duty vehicle charging,'' IEEE Trans. Transport Electrific., vol. 7, no. 3, pp. 1205–1218, Sep. 2021, doi: 10.1109/TTE.2021.3049138.

[13] S. A. Gorji, H. G. Sahebi, M. Ektesabi, and A. B. Rad, ''Topologies and control schemes of bidirectional DC–DC power converters: An overview,'' IEEE Access, vol. 7, pp. 117997–118019, 2019.